Desalination and Water Treatment
www.deswater.com
37(2012)337–349
January
1944-3994/1944-3986
doi: 10/5004/dwt.2012.2599
Taylor & Francis
Taylor & Francis Group

Flue gas desulfurization and humidification dehumidification in power plants

R.S. Ettouney[a,*], N.A. Fawzi[b], M.A. El-Rifai[a], H.M. Ettouney[b]

[a]*Chemical Engineering Department, Cairo University, Egypt*
[b]*Chemical Engineering Department, Kuwait University, Kuwait*
Email: ettouney@hotmail.com

Received 22 January 2011; Accepted 10 August 2011

ABSTRACT

Performance evaluation is presented for flue gas desulfurization (FGD), humidification and dehumidification desalination (HDD) of flue gases emitted from power plants. The proposed system is based on use of seawater for SO_2 absorption and removal from the flue gases. The FGD and HDD processes are separated in order to achieve the highest possible efficiency. This is because FGD requires low temperatures to achieve high rates of absorption and removal of SO_2. On the other hand, HDD requires higher temperatures to provide sufficient temperature difference and driving force for humidification and dehumidification. Analysis of both systems is applied to the emission rate data of power plants in Kuwait. The design results of the seawater SO_2 absorption column showed variations in the column height between 8.1–12.6 m as the power plant capacity was increased from 244–4173 MW. Analysis of the HDD system show that it might not be the optimum desalination alternative because of its limited production capacity. However, the process layout is simple and can be formed of two packed columns for humidification and dehumidification, which requires a small capital when compared to conventional thermal or membrane desalination.

Keywords: Flue gas desulfurization; Absorption; Humidification; Dehumidification; Modeling; Desalination

1. Introduction

The humidification dehumidification desalination (HDD) process remains to be limited to experimental and prototype scale. Review of desalination market data show that commercial processes are the multistage flash (MSF), reverse osmosis (RO), multiple effect evaporation (MED), and single effect mechanical vapor compression (MVC) [1]. Irrespective of this, the HDD process is thought by several researchers and investigators as a simple technology that can provide for remote areas and small communities with a sustainable source of desalinated water. More efficient form of the HDD process was made through the use of multiple effect configurations (known as MEH).

The review presented by Parekh et al. confirmed that the HDD process requires additional developments to reduce power consumption and to increase productivity [2]. The economics review of Al-Hallaj et al. on the performance of HDD combined with solar collectors showed that the most critical element in process commercialization is the minimization of the area of the humidifier, dehumidifier, and solar collector [3].

Several studies are found in the literature on modeling and performance evaluation of the multiple effects HDD. In this configuration the air stream is humidified and heated in a multi effect system in order to increase its absolute humidity. Yuan and Zhang modeled the performance of a two effect HDD system combined with solar collectors [4]. The modeling was based on ambient conditions of Xi'an, China. Results show specific

*Corresponding author.

productions, which are based on the area of the solar collector, of 2.7–5.2 kg/(m^2 d). Yamali and Solmus showed that the productivity of an HDD system increases by 30% upon the adoption of a double solar heater for the intake air [5,6]. A maximum productivity of 3.5 kg/(m^2 d), which was based on the area of the air solar heaters, was obtained for the summer condition in Ankara, Turkey. This result was based on the area of the air solar heater. Orfi et al. and Marmouch et al. studied the performance of the HDD process combined with solar collectors for air and water [7,8]. The developed model was applied to the ambient conditions in Tunis. Production rates in a single effect system were reported at values greater than 15 kg/(d m^2). Use of multiple effect system resulted in the increase in the production rates by 22 kg/(d m^2) [7,8].

Houcine et al. tested and modeled a pilot scale multiple effect HDD unit [9]. The system included four humidification effects and four dehumidification effects. Daily production rates of 355 kg were reported for the ambient conditions of Tunis.

Recent studies on HDD systems include modeling, optimization, and novel cycles. Narayan et al. developed a comprehensive model for the HDD system, which included mass, energy, and entropy balances [10–16]. Several novel cycles were proposed by the authors and showed that these cycles provide gain output ratio in excess of 5, which is much higher than conventional HDD. Li et al. showed that use of the HDD process can play a major role in treatment of industrial wastewater with possibility for 20% recovery and more than 99% salt rejection [14]. This was illustrated through the use of a small scale HDD unit (7.5 l/d) which produced water from natural gas production. Soufari et al. showed that system optimization before actual construction results in increase of productivity from 2% to more than 4% [15]. This finding was reported for a small system with a productivity of 240 l/d. Recent evaluation of small scale solar HDD system (1000 l/d) was reported by Mathioulakis et al. [16]. The review showed that the water production cost remains high, absence of system standards and manufacturing companies. On the other hand, the main attractive feature of the system is its simplicity and possible use of generated heat for other uses.

The most common FGD system is based on wet scrubbing, where an aqueous solution or slurry of alkaline compounds is used to absorb and react with the sulfur dioxide gas. The alkaline compounds include lime, limestone, magnesium oxides, magnesium hydroxide, sodium sulfite, and sodium hydroxide. Fortunately, all of these compounds are found in seawater. Therefore seawater FGD is very attractive for the following facts [17–19]: 1) The process requires seawater only and no additional chemicals, 2) The rejected water, which includes sulfate salts, can be reacted with ammonia to generate ammonium sulfate, a rich fertilizer in nitrogen and sulfur, 3) Precipitates from the desulfurization process can be used for land reclamation from the sea, and 4) The process can be used to control emission rates of other pollutants, which includes NOx, CO_2, CO, and SO_3.

Most of the literature studies on FGD using seawater focused either on discussion and description of the process features and merits or on study and analysis of the process kinetics. Abrams et al. developed a new a process to remove more than 90% of SO_2 from flue gas using seawater and calcite lime, which contain soluble magnesium, this eliminates scaling in the scrubber system and reduces the operating cost [20]. Most importantly, the process has a negligible impact on the environment. This is because the effluent water stream contained gypsum at low concentrations; therefore, no sludge or solid waste was generated. Moreover, the effluent contained no toxic or harmful compounds and it is suitable for direct discharge to the sea. Oikawa, et al. discussed promising and attractive features for use of seawater from cooling system in power plants located on sea shores to scrub sulfur dioxide from flue gases [21]. The study presented several design configurations for FGD using seawater and was applied to a 600 MW power plant in China.

Zhao et al. studied the kinetics of SO_2 absorption and reaction in seawater [22]. The results showed that factors affecting SO_2 absorption in seawater include alkaline, ion intensity, catalysis of Cl^- and transition metal ions Fe, Mn. The effect of alkalinity is greater than the catalysis of Cl^-, Fe2+ and Mn is greater than ion intensity. The mechanisms of catalysis oxidation for S(IV) by Cl, Fe and Mn was explained and a number of measures were discussed to improve the desulfurization process.

Ortez et al. and Vidal et al. studied oxidation kinetics of sulfur by means of a commercially available activated carbon [23,24]. The study was extended to a pilot scale unit to demonstrate the high-efficiency of structured packing, which reduced the seawater flow rate by 47% and the production cost by 33%. With the appropriate activated carbon, it is possible to reach a greater oxidation rate at a low pH level than by operating conventionally at a high pH level without a catalyst A.

There are no available studies in the open literature on combined systems of flue gas desulfurization (FGD) and HDD. The available studies focus on use of the flue gas to generate low grade energy for operation of MED and MSF [25–27]. Cohen et al. discussed the feasibility of generating energy for 8,500–10,000 m^3/d desalination systems using waste heat from flue gases [25]. The economic analysis of this proposed process showed competitiveness of the production cost against conventional thermal desalination plants. A similar conclusion was made by Sommarva for combined systems of flue

gas heating with conventional MSF/MED systems [26]. Dajnak and Lockwood gave an initial assessment of this concept and concluded that useful quantities of fresh water can be produced [27]. Further studies are required to optimize the waste to water conversion and to assess the economy of the concept relative to competing desalination energy sources.

This study focuses on modeling and analysis of the combined system of FGD and HDD. The proposed model is applied to the operating conditions of the power plants in Kuwait. This is motivated by the large capacity of these plants and the use of high sulfur oil fuels. The analysis includes sizing of the required FGD and HDD units, studying the performance characteristics of both units, and evaluating the amounts of water generated relative to desalination capacity in Kuwait.

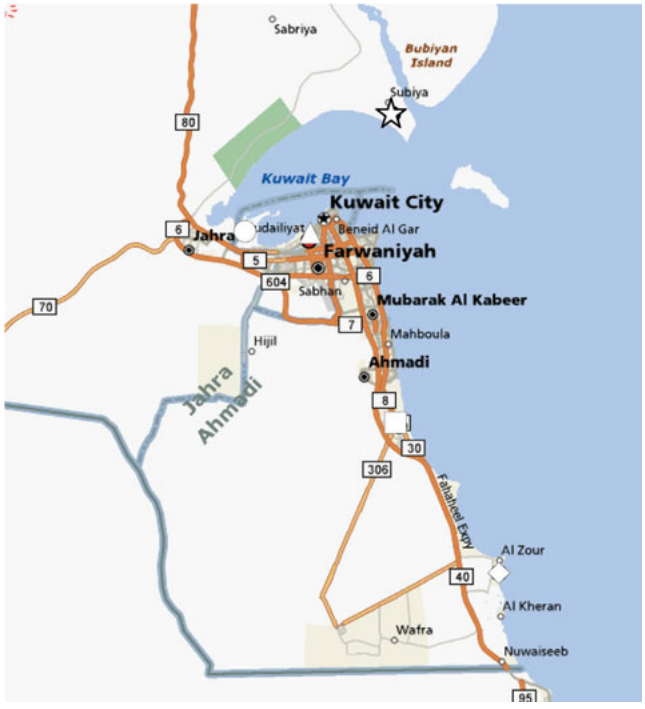

Fig. 1. Map of the State of Kuwait showing locations power plants (☆: Saubiya, ○: Doha East and West, Δ: Shuwaikh, □: Shuaiba north and south, ◊: Azzor north and south) relative to population and industrial area.

2. Power plants in Kuwait

Kuwait city extends over the shore line of the Gulf with a population around 2 MM inhabitants. There are eight major power plants in Kuwait, see Fig. 1. The power capacity is designed to meet the high consumption rate of electricity during the summer time to operate indoor air conditioning units. This may account for more than 70% of the total power capacity of 16,095 MW. Another major power consumer is the desalination plants, which are located in all locations.

Table 1 shows the power capacity for each of the eight locations together with estimates for pollutant emissions, which includes SO_2, NOx, CO_2, and particulate matter (PM). Emissions rates of SO_2, NOx, CO_2, and PM are 6, 1.8, 600, and 0.05 kg/MWh. These values are based on the rates reported by the US-EPA (www.epa.gov). Emissions of H_2O and total emissions were obtained by performing stoichiometric calculations that assumed a fuel composition of (C: 82.8, H:12.19, O:2.15, S:2.8, in mass % and the balance is ash) and 25% excess air.

3. FGD and HDD process diagram

The proposed scheme for simultaneous FGD and HDD for flue gases of power plants is shown in Fig. 2. As shown the flow diagram addresses the problem that FGD requires lower temperature than HDD in order to achieve high level of sulfur removal. Separation of the two processes requires the use of a heat exchange

Table 1
Emission rates of the power plants in Kuwait

Location	Power (MW)	SO_2 (kg/hr)	NOx (kg/hr)	CO_2 (kg/hr)	H_2O (kg/hr)	PM (kg/hr)	Total* (kg/hr)
Saubiya	4173	25038	7511.4	2503800	904782.27	208.65	10155679
Azzor North	2500	15000	4500	1500000	542045.45	125	6084159
Azzor South	3511	21066	6319.8	2106600	761248.64	175.55	8544593
Shuaiba South	720	4320	1296	432000	156109.09	36	1752238
Shuaiba North	1179	7074	2122.2	707400	255628.64	58.95	2869289
Doha East	1158	6948	2084.4	694800	251075.45	57.9	2818183
Doha West	2610	15660	4698	1566000	565895.45	130.5	6351862
Shuwaikh	244	1464	439.2	146400	52903.636	12.2	593814

*Total emissions do not include particulate matter (PM) and are based on 25% excess air, fuel composition of (C: 82.8, H:12.19, O:2.15, S:2.8, in mass % and the balance is ash). The resulting mole fraction of H_2O, CO_2, NOx, SO_2, O_2 and N_2 in the flue gases are (8.0314×10^{-2}, 9.0922×10^{-2}, 2.728×10^{-4}, 1.1153×10^{-3}, 0.16617, 0.6611).

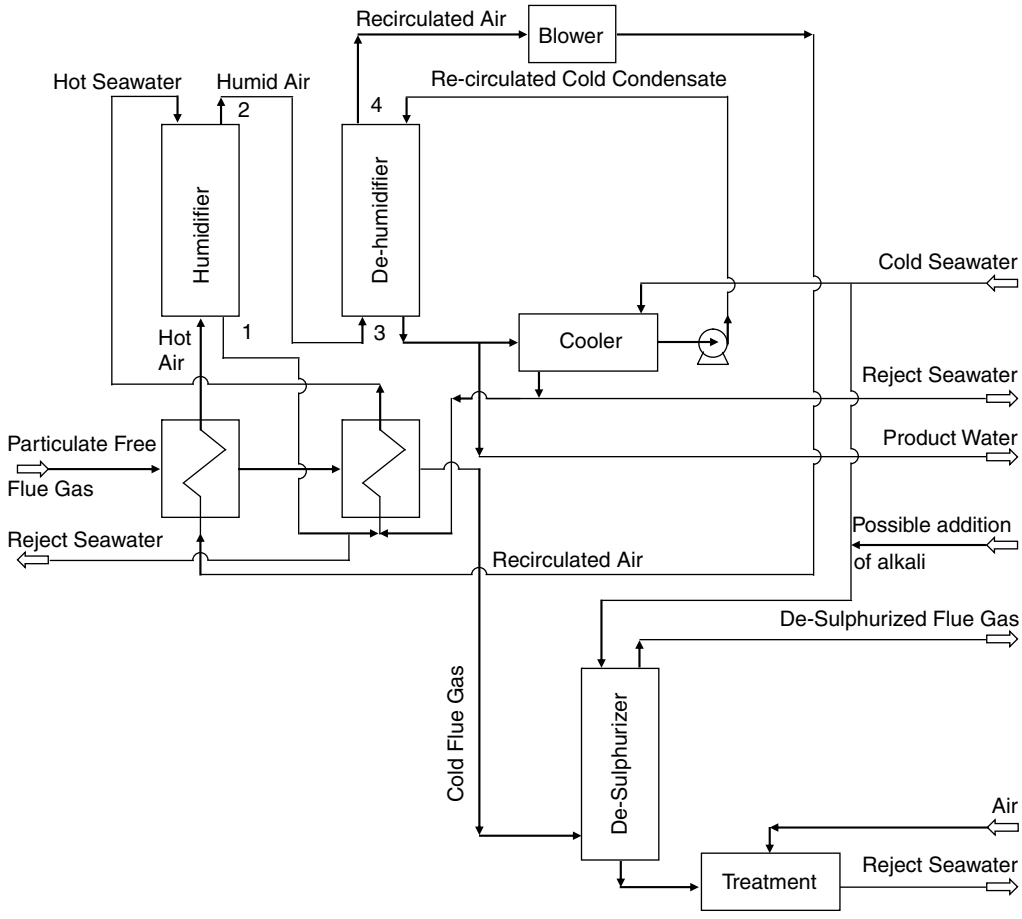

Fig. 2. Schematic of the FGD and HDD processes.

unit, where the flue gases are cooled from 150°C to 50°C before entering the seawater absorption column [28–33]. This energy is recuperated by ambient air and feed seawater which are used in the HDD system. It should be noted that gas-gas heat exchangers are the most costly in heat transfer equipment. However, their use is common in power plants for preheating of intake air and cooling of flue gases.

As shown in Fig. 2, the heated ambient air and sea water enter the humidifier of the HDD system at a temperature of 80°C. At these conditions evaporation from the water stream might be large; however, examination of typical operating conditions where the inlet/outlet air temperatures in the humidifier are 80 and 50°C, respectively, and the corresponding inlet/outlet absolute humidities of the air are 0.0615 and 0.105 kg H_2O/kg dry air, respectively. Assuming that flow rate of dry air and water are 1 kg/s and 2 kg/s, respectively, would give an evaporation rate of 0.044 kg/s. Therefore, the total loss in the water flow rate is approximately 2.2%. The humidifier is a counter-current packed column that includes packing blocks with heights limited to 1 m. This is to insure good distribution and contact of air and water. The dehumidification process of the humidified air takes place in a counter-current packed column or a shell and tube condenser. Dehumidification is made between the humidified air and part of the product distillate water. The dehumidified air is circulated through the system, where it is preheated against the flue gases prior to being admitted to the humidifier. The intake seawater is divided into two streams. The first is preheated in a heat exchanger against the distillate product and the second is used in the FGD absorption column. Part of the seawater leaving the cooler is rejected back to the sea and the remaining part is preheated against the flue gases prior to being admitted in the humidifier.

The absorption water rejected from the FGD column is treated prior to disposal back to the sea. The absorption model developed by Abdulsatar et al. indicates that the absorbed SO_2 gas hydrolyzes in seawater much faster than pure water [28]. SO_2 forms HSO_3^- ions, which are weak and dissociate into SO_3^{--}. Blowing air into the treatment tank results in the formation of soluble ions of $NaSO_4^-$ and KSO_4^- and sparingly soluble $MgSO_4$, $CaSO_3$, and $CaSO_4$.

4. Model of FGD and HDD

The main assumption of the FGD absorption column is linearity of the equilibrium and operating lines. This is strongly motivated by the low concentration of SO_2 in the flue gases. Therefore, the model for the number and height of a transfer unit in the absorption column is obtained in a closed form relation as given below to determine the height of the absorption column:

- Number of transfer units

$$N_{OG} = \frac{1}{1 - 1/AF} \ln\left(\frac{1}{RR}\left(1 - \frac{1}{AF}\right) + \frac{1}{AF}\right) \quad (1)$$

where $RR = \frac{(y_{SO_2})_2}{(y_{SO_2})_1}$.

- Height of a transfer unit

$$H_{OG} = \frac{M_a}{k_y' a\ S\bar{M}_a} + AF\frac{M_w}{k_x' a\ S\bar{M}_a} \quad (2)$$

where $k_x' a = 0.152\left(\frac{M_w}{S}\right)^{0.82}$ and $k_y' a = 0.0594\left(\frac{M_a}{S}\right)^{0.7}\left(\frac{M_w}{S}\right)^{0.25}$ [34].

- Height of absorption column

$$z = H_{OG} N_{OG} \quad (3)$$

Solution of the FGD model requires definition of the equilibrium line slope (m) for absorption of SO_2 in seawater at atmospheric conditions and the desired operating temperature. Also, the removal rate (RR) of SO_2 from the flue gases and the flow rate of absorption water (M_a).

There are two elements in the HDD system, which are the humidifier and the dehumidifier. The model of both units is similar and is based on the following assumptions:

- Steady state operation
- Negligible heat losses to the surroundings.
- Constant specific heat at constant pressure for the dry air and water vapor.
- The air water interface is assumed at saturation.
- Water evaporation into the air stream has negligible effect on the total flow rates of the water and air streams.
- Absorption of air components has negligible effect on the total flow rates of the air and water streams.

Based on the above assumptions and following the standard development of the material and energy balances inside a humidification column gives the following relation [35]:

$$z = \frac{M_a}{K_y a\ S}\int_{Hy_1}^{Hy_2}\frac{dHy}{(Hy_i - Hy)} \quad (4)$$

Eq. (4) is solved analytically following the development given in Appendix A, which is based on expressing Hy_i and Hy in terms of the temperature at the air water interface within the humidification column [35]. Therefore, the integration given in Eq. (4) is reduced to

$$z = \frac{M_a}{K_y a\ S}\int_{T_{wi_1}}^{T_{wi_2}}\frac{(c_2 + c_3 T_{wi})\ dT_{wi}}{b_1 + b_2 T_{wi} + b_3 T_{wi}^2} \quad (5)$$

The temperatures of the air water interface at column top and base are given in terms of slope of the lines connecting the equilibrium curve and the operating line. These relations are as follow:

$$T_{wi_2} = T_{w_2} - \frac{Ky\ a}{h_L\ a}(Hy_2 - Hy_{2_i}) \quad (6)$$

$$T_{wi_1} = T_{w_1} - \frac{Ky\ a}{h_L\ a}\left(Hy_1 - Hy_{1_i}\right) \quad (7)$$

Eqs. (6) and (7) require iterative solution prior to integration of Eq. (5) in order to define the inlet and outlet temperatures of the air/water interface. Eq. (5) is integrated analytically following the procedure given in appendix B.

Calculations of the height of the humidification column using the integral of Eq. (5) requires definition of the air flow rate (M_a), the water flow rate (M_w), the inlet and outlet water temperatures (T_{w_2} and T_{w_1}), the specific heat at constant pressure for water vapor and dry air (Cp_a, Cp_v), inlet air temperature (T_{a1}), diameter of the humidification column (D_h), the overall mass transfer coefficient of water in air ($K_y a$), and the heat transfer coefficient between the water and air phases ($h_L a$).

Appendix A includes correlations used to evaluate the saturation pressure of water (P^*), the latent heat of water evaporation (λ), the air enthalpy at saturation conditions (Hy^*), and the specific heat at constant pressure of liquid water (Cp_w).

The dehumidifier model is similar to the humidifier model. However, the enthalpy of dry air is higher than the saturation enthalpy, which is measured at the air/water interface. Therefore, Eq. (4) is changed to the following form:

$$z = \frac{M_a}{K_y a\ S} \int_{Hy_3}^{Hy_4} \frac{dHy}{(Hy - Hy_i)} \quad (8)$$

Calculations of the height of the dehumidification column using the integral of Eq. (8) requires definition of the air flow rate (M_a), the water flow rate (M_w), the inlet and outlet water temperatures (T_{w_4} and T_{w_3}), the specific heat at constant pressure for water vapor and dry air (Cp_a, Cp_v), inlet air temperature (T_{a_3}), diameter of the dehumidification column (D_d), the overall mass transfer coefficient of water in air ($K_y a$), and the heat transfer coefficient ($h_L a$).

In most of the literature studies, air dehumidification is achieved in a shell and tube condenser. In this case, the cooling water is routed on the tube side and the humid air on the shell side. Finned tubes can be used to increase the overall heat transfer coefficient [36].

The condenser model includes two equations, which are the energy balance and the heat transfer equations [37]. These equations are given by the following relations:

$$M_{cw} Cp_w (T_{w_3} - T_{w_4}) = M_a (Hy_3 - Hy_4) \quad (9)$$

$$M_{cw} Cp_w (T_{w_3} - T_{w_4}) = U_c A_c LMTD_c$$
$$M_{pw} = M_a (H_3 \quad H_4) \quad (10)$$

where, *LMTDc* is the condenser logarithmic mean temperature difference (°C), which is given by the relation:

$$LMTD_c = ((T_{a_3} - T_{w_3}) - (T_{a_4} - T_{w_4}))/\ln\left(\frac{T_{a_3} - T_{w_3}}{T_{a_4} - T_{w_4}}\right) \quad (11)$$

Calculations of the heat transfer area of the condenser and flow rate of cooling water using Eqs. (9) and (10) requires definition of the inlet and outlet air and water temperatures (T_{w_3}, T_{w_4}, T_{a_3}, T_{a_4}), the overall heat transfer coefficient (U_c), the inlet and outlet absolute humidity of air (H_3, H_4), and the inlet air flow rate.

The production rate of fresh is determined by obtaining the difference of the mass flow rate of the input and output air humidity. This relation is given by

$$M_{pw} = M_a\ (H_3 - H_4) \quad (12)$$

In this relation, M_a is the mass flow rate of dry air and H_3 and H_4 are the inlet and outlet absolute humidities of the air stream, respectively.

5. Results and discussion

Variations of height of the FGD absorption column are shown in Table 2 as a function of the power plant capacity. These results are obtained for SO_2 removal ratio (*RR*) of 0.1 and a column diameter of 3 m, which gives a cross section area (*S*) of 7.068 m^2. Also, the slope of the equilibrium line is assumed equal to 25 with units equal to the ratio of the SO_2 mole fractions in gas and liquid phases. In these calculations the flow rate of the absorption seawater is adjusted to obtain a constant ratio of 1.2 for the factor ($M_w/(m\ M_a)$). As a result, the value of the number of transfer units (N_{OG}) is similar for all power stations with a value of 5.5. Also, it should be noted that the results shown in Table 2 are the theoretical values. Therefore, use of actual absorption efficiencies which may vary over a range of 25–50% would increase the column height by a factor of 2–4.

Effect of varying the diameter of the absorption column and the removal ratio on the absorption column height are shown in Fig. 3. As would be expected and at constant gas flow rate increase in the column diameter would reduce the column height. Similarly, reduction in the removal ratio would also reduce the column height. Fig. 4 shows variations in the column height as a function of the absorption factor ($M_w/m\ M_a$) and the equilibrium constant (*m*). As shown, varying the equilibrium constant from 20–30 has negligible effect on the column diameter. On the other hand, the absorption factor has more sizeable effect, where the column

Table 2
Height of absorption column for SO_2 removal from flue gases

	Saubiya	Azzor N.	Azzor S.	Shuaiba S.	Shuaiba N.	Doha E.	Doha W.	Shuwaikh
P (MW)	4173	2500	3511	720	1179	1158	2610	244
M_a (kg/s)	2821.0	1690.0	2373.5	486.7	797.0	782.8	1764.4	164.9
M_w (kg/s)	84630.7	50701.3	71204.9	14602.0	23910.7	23484.9	52932.2	4948.4
N_{OG}	5.5	5.5	5.5	5.5	5.5	5.5	5.5	5.5
$ky'\ a$ (kg mole/s m^3)	5.1	3.1	4.3	1.0	1.5	1.5	3.3	0.3
$kx'\ a$ (kg mole/s m^3)	55.4	36.4	48.1	13.1	19.6	19.4	37.7	5.4
H_{OG} (m)	1.4	1.3	1.4	1.1	1.2	1.2	1.3	0.9
z (m)	7.8	7.2	7.6	6.0	6.4	6.4	7.2	5.1

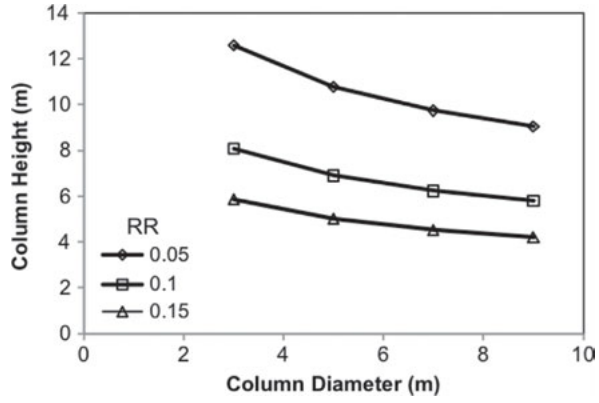

Fig. 3. Variations in the height of the SO_2 seawater absorption column in Shuwaikh power plant as a function of the column diameter and SO_2 removal ratio. Calculations are made for equilibrium constant of 25 and absorption factor of 1.2.

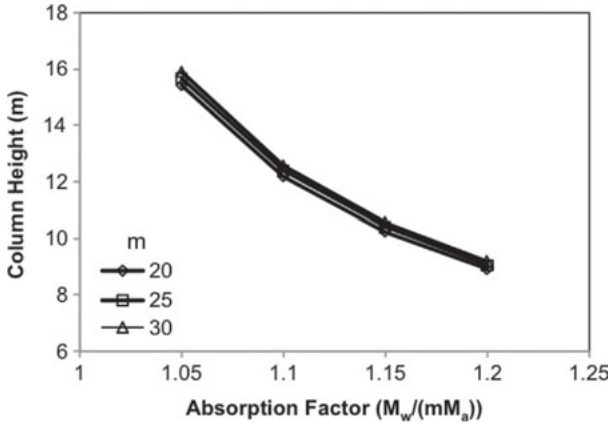

Fig. 4. Variations in the height of the SO_2 seawater absorption column in Shuwaikh power plant as a function of the equilibrium constant and absorption factor. Calculations are made for a column diameter of 9 m and removal ratio of 0.05.

height is reduced by a factor of two as the parameter is increased from 1.05–1.2. This increase is associated with a similar increase in the water flow rate because the flow rate of the flue gases are kept constant in all calculations.

Design parameters and results of the HDD system for various power plants in Kuwait are summarized in Tables 3 and 4, respectively. As shown in Table 4, the diameters of the humidifier and dehumidifier are adjusted in order to maintain the column height within practical limits. It should be noted that the units with large diameters can be divided into several units with smaller diameters. The total amount of fresh water produced from all power plants is equal to 91,919 m^3/d. This amount is less than 10% of the production of all desalination plants in Kuwait, which averages 1×10^6 m^3/d.

Table 3
Design data for the HDD system

Parameter	Value
T_{w_2} (°C)	62
T_{w_1} (°C)	60
T_{w_3} (°C)	30
T_{w_4} (°C)	30
T_{a_1} (°C)	80
T_{a_3} (°C)	36
Cp_w (J/kg dry air K)	4180
Cp_a (J/kg dry air K)	1005
Cp_v (J/kg H_2O K)	1880
Y_{w_1}	0.09
$Ky\,a$ (kg/s m^3)	0.354
U_c (kW/m^2 K)	0.1
z_c (m)	10
D_c (m)	0.03
T_{cw_4} (°C)	30
(M_w/M_a)h	2
(M_w/M_a)d	4

Sensitivity of the HDD model to various design parameters is shown in Figs. 5 and 6. All calculations are made for the Shuwaikh power plant conditions (see Table 1) and the HDD design parameters given in Table 3. As shown in Fig. 5, the height of the humidification column is very sensitive to the increase in both the temperature drop of the cooling water and the water (at point 2 in Fig. 2) to air (at point 1 in Fig. 2) mass flow rate ratio. Increase of either parameter increases the thermal load of the cooling tower; therefore, larger height is needed to achieve the required degree of cooling. The results shown in Fig. 6 indicates that the increase in the height of the humidification column is more sensitive to the increase in the inlet mass fraction of water vapor in the air stream than to the increase in the air temperature. This is because increase in the inlet temperature of the air stream affects only the tower thermal load of the sensible heat of the air stream. On the other hand, increase in the inlet mass fraction of H_2O in the inlet air stream affects both the sensible and the latent heat terms. In this regard, the thermal load for removal of the latent heat of water condensation is much larger than the thermal load for removal of the air sensible heat.

Variations in the height of the dehumidification column as a function of the inlet water temperature, outlet air temperature, column diameter, and water to air mass flow rate ratio are shown in Figs. 7 and 8. As shown in Fig. 7, the column height is sensitive to both the column diameter and the inlet air temperature. Decrease in the column height with increase of the column diameter is

Table 4
Design characteristics of the HDD for power plants in Kuwait, obtained at T_{w_4} = 36°C and T_{a_2} = 48.7°C

	Saubiya	Azzor S.	Doha W.	Azzor N.	Doha E.	Shuaiba N.	Shuaiba S.	Shuwaikh
M_a (kg/s)	7000.2	5889.7	4378.3	4193.8	1942.5	1977.8	1207.8	409.3
M_w (kg/s)	14000.4	11779.4	8756.6	8387.5	3885.1	3955.5	2415.6	818.6
D_h (m)	12.0	12.0	10.0	10.0	6.0	6.0	6.0	3.0
z_h (m)	11.6	9.8	10.4	10.0	12.9	13.1	8.0	10.9
D_d (m)	50.0	50.0	40.0	40.0	30.0	30.0	30.0	15.0
z_d (m)	12.8	10.8	12.5	12.0	9.9	10.1	6.2	8.3
z_c (m)	36.2	33.2	28.7	28.0	19.1	19.3	15.0	8.8
A_c (m^2)	908,562.6	764,429.2	568,259.8	544,310.2	252,124.5	256,696.7	15,6761.3	5,3124.7
M_d (m^3/d)	25,238.2	21,234.4	15,785.2	15,119.9	7,003.6	7,130.6	4,354.5	1,475.7
M_{cw} (m^3/d)	2,558,079.9	2,152,269.0	1,599,949.3	1,532,518.5	709,862.6	722,735.7	441,365.3	149,573.8

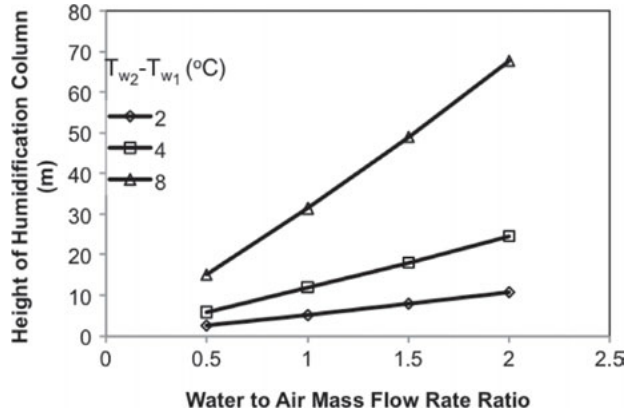

Fig. 5. Variations in the height of the humidification column in Shuwaikh power plant as a function of air to water mass flow rate ratio and temperature drop in the cooling water.

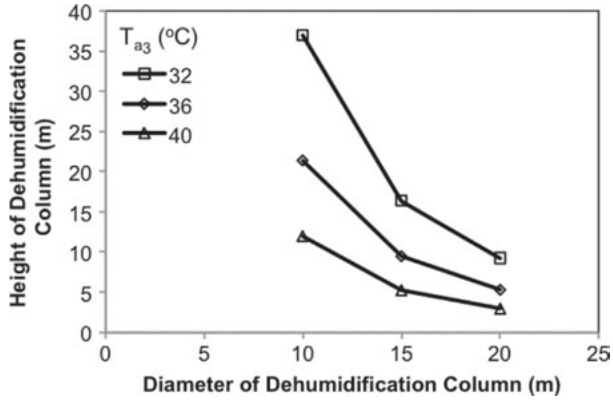

Fig. 7. Variations in the height of the dehumidification column in Shuwaikh power plant as a function of outlet air temperature and column diameter.

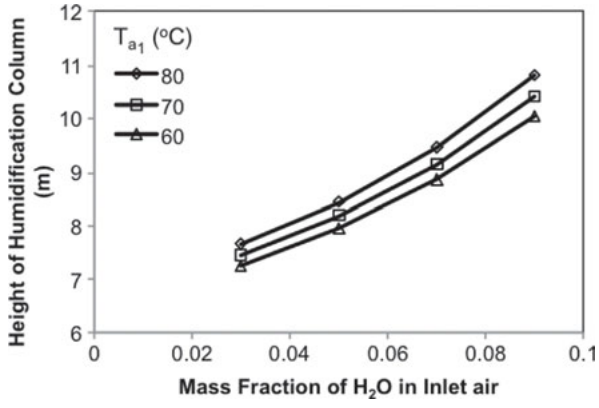

Fig. 6. Variations in the height of the humidification column in Shuwaikh power plant as a function of mass fraction of H_2O in inlet air and inlet air temperature.

caused by the decrease of the specific energy per unit cross section area of the column. Similarly, decrease in the column height with the increase in the outlet air temperature is a result of the decrease in the thermal load of column.

Fig. 8 shows variations in the height of the dehumidification column as a function of water to air mass flow rate ratio and the inlet water temperature. It should be noted that the dehumidification column works as a condenser; therefore, increase of the water flow rate on the tube side would increase its thermal capacity and as a result smaller column is required. Similarly, decrease in the inlet water temperature increases the thermal capacity of the water stream and the driving force for heat transfer; therefore, the column height decreases with the decrease in the inlet water temperature.

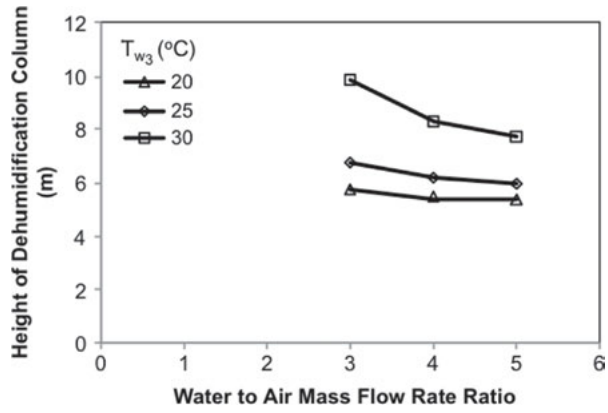

Fig. 8. Variations in the height of the dehumidification column in Shuwaikh power plant as a function of inlet water temperature and the water to air mass flow rate ratio.

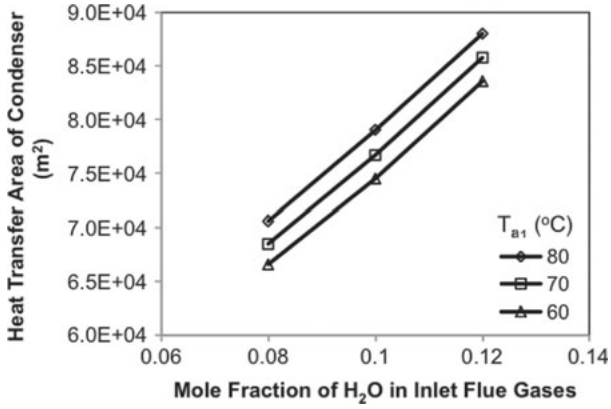

Fig. 9. Variations in the heat transfer area of the condenser in Shuwaikh power plant as a function of the mass fraction of H_2O in inlet air and inlet air temperature.

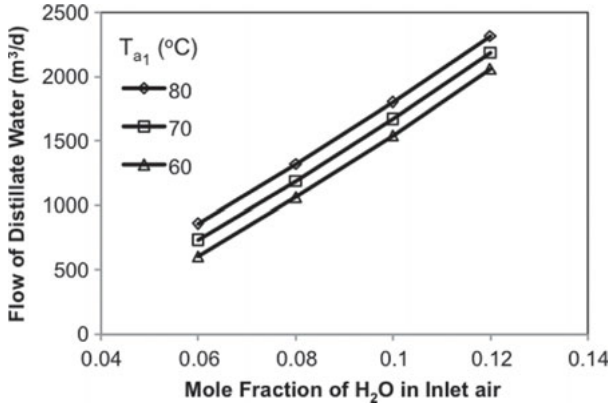

Fig. 10. Variations in the distillate flow rate in Shuwaikh power plant as a function of mass fraction of H_2O in inlet air and inlet air temperature.

Fig. 9 shows variations heat transfer area of the humidifier that has a shell and tube configuration and as modeled by Eqs. (10) and (11). The figure shows variations in the condenser heat transfer area as a function of the inlet mass fraction of H_2O in the inlet flue gases and the inlet temperature of the flue gases are shown in Fig. 9. As shown the condenser heat transfer area increases with the increase in the inlet mass fraction of H_2O and the inlet temperature of the flue gases. As mentioned before the effect of the increase in the inlet mass fraction of H_2O is more sizeable than the effect of the increase in the inlet flue gases temperature. This is because the inlet mass fraction of H_2O affects both the sensible and latent heats of the system. This results in a larger increase in the system thermal load and hence the increase in the heat transfer area of the condenser is more pronounced.

Variations in the system production capacity of fresh water are shown in Fig. 10 as a function of the same parameters shown in Fig. 9. As shown, the production capacity increases with the increase in the inlet mass fraction of H_2O and the inlet temperature of the flue gases. Increase in the production capacity is caused by maintaining constant temperature for the outlet air from the condenser. The driving force for water production as shown by Eq. (12) increases with the increase in the temperature and absolute humidity of the air to the condenser.

6. Conclusions

A system was proposed for FGD and HDD of flue gases emitted from power plants in Kuwait. The main feature of the proposed system is the separation of the FGD and HDD systems. This is because FGD requires operation at low temperatures in order to maximize SO_2 removal. On the other hand, HDD requires high temperature operation to obtain the largest possible amount of fresh water. Also, the proposed HDD process used ambient air instead of flue gases. This was found necessary to prevent possibility of contamination of the product distillate water with acid gases and other pollutants.

Mathematical models were developed to obtain design and performance characteristics for the proposed systems. Results for design of the FGD system show high sensitivity in variations in the height of the absorption column to the removal rate of SO_2 and the absorption factor (AF). On the other hand, it was found that the height of the absorption column is less sensitive to variation in the equilibrium constant and diameter of the column. The design data for all power plants in Kuwait show feasible height for the absorption column which varies between 8.1–12.6 m as the power capacity

is increased from 244–4173 MW. This finding indicates that it is not necessary to operate at higher pressure as proposed by Pipitone and Bolland [29].

Design and performance evaluation of the HDD process show the need to operate the humidifier at low water to gas flow ratio and small temperature drop in the cooling water, which reduces the required height. To maximize water production (in either a packed bed dehumidifier or a shell and tube condenser) it is necessary to operate that unit at high temperatures and high water vapor mole fraction in the inlet air stream in the dehumidifier. However, increase in both parameters results in larger heat transfer area in the condenser. Therefore, it is necessary to optimize the values of these parameters in order to obtain the design characteristics for the most efficient configuration.

A critical finding in this study is the small production capacity of the HDD system. The total amount of desalinated water from all power plants in Kuwait is found to be less than 10% of total production capacity of all desalination plants in Kuwait, which averages 1×10^6 m^3/d. This finding is consistent with industrial practice, where MSF, MED, or RO are the industrial standard; while HDD is limited to studies of conceptual design or laboratory scale units.

Appendix A: Physical and thermodynamic correlations

Saturation pressure (p^*)

The saturation pressure of water is given by the following correlation [40]

$$p^* = EXP(f_1/T + f_2 + f_3 \times T + f_4 \times T^2 + f_5 \times T^3 + f_6 \times LN(T)) \times 0.001$$
$$\lambda = 2501.897149 - 2.407064037\ T + 1.192217 \times 10^{-3}\ T^2 - 1.5863 \times 10^{-5}\ T^3 \quad (A.1)$$

where p^* is in kPa and T in K. The constants f_1–f_6 are given in the following table

f_1	f_2	f_3	f_4	f_5	f_6
–5.80E+03	1.391499	–4.86E–02	4.18E–05	–1.45E–08	6.545967

The latent heat for water evaporation

The latent heat for water evaporation is given by the following relation [40]

$$\lambda = 2501.897149 - 2.407064037\ T + 1.192217 \times 10^{-3} T^2 - 1.5863 \times 10^{-5} T^3 \quad (A.2)$$

where λ is in kJ/kg and T in °C.

Air enthalpy at saturation temperature (Hy^*)

The expression for the air enthalpy at saturation was obtained by fitting saturation enthalpy against the saturation temperature

$$H_y^* = 155051 - 10865.85\ T + 269.023\ T^2$$
$$Cp = \left(\begin{matrix} 4206.8 - 1.1262\ T + 1.2026 \times 10^{-2}\ T^2 \\ +\ 6.8777 \times 10^{-7}\ T^3 \end{matrix} \right) \left(10^{-3}\right) \quad (A.3)$$

where Hy^* is in J/kg dry air and T is in °C.

The water specific heat at constant pressure

The specific heat at constant for water is given by the following relation [40]

$$Cp = \left(\begin{matrix} 4206.8 - 1.1262\ T + 1.2026 \times 10^{-2}\ T^2 \\ +\ 6.8777 \times 10^{-7}\ T^3 \end{matrix} \right) \left(10^{-3}\right) \quad (A.4)$$

where Cp is kJ/(kg°C), T is in °C.

The overall heat transfer coefficient of the condenser

The correlation of the overall heat transfer coefficient is based on the well known Ditus-Bolter Eq. [38] and the correlation of the heat transfer coefficient on the air side reported by Al-Sahali and Ettouney [39]. These two equations are

$$h_{cw} = 0.023(Re_{cw})^{0.8}(Pr_{cw})^{0.333}(k_{cw}/d_i) \quad (A.5)$$

$$h_a = 1.019 \times 10^{-14}(Re_a)^{0.4806}(Pr_a)^{-95.69}(k_a/d_0) \quad (A.6)$$

The overall heat transfer coefficient is then obtained from the relation

$$\frac{1}{U_c} = \frac{1}{h_a}\frac{r_o}{r_i} + \frac{1}{h_{cw}} + \frac{r_i}{k_w} \ln \frac{r_0}{r_i} \quad (A.7)$$

Appendix B: Integration constants of the humidification column

Development of Eq. (5) requires definition of the terms (Hyi-Hy), Hy, and dHy in terms of the air/water interface temperature. This is made through the use of the slope of the lines connecting the equilibrium curve and the operating line, which is given by:

$$-\frac{h_L\ a}{Ky\ a} = \frac{Hy_i Hy}{T_{wi} - T_w} \quad (B.1)$$

and the operating line equation

$$\frac{Hy - Hy_1}{T_w - T_{w_1}} = \frac{M_w Cp_w}{M_a} \tag{B.2}$$

Using the correlation for Hy_i (Eq. (A.3)) or $Hy_i = a_1 + a_2 T_{wi} + a_3 T_{wi}^2$, and combining Eqs. (B.1) and (B.2) to eliminate T_w would give an explicit form for Hy as a function T_{wi}, which is given by

$$Hy = A_1 + A_2 T_{wi} + A_3 T_{wi}^2 \tag{B.3}$$

where

$$A_1 = \frac{1}{\dfrac{M_a}{M_w Cp_w} + \dfrac{Ky\ a}{h_L\ a}} \left(a_1 \frac{Ky\ a}{h_L\ a} - Hy_1 \frac{M_a}{M_w Cp_w} - T_{w_1} \right) \tag{B.4}$$

$$A_2 = \frac{1}{\dfrac{M_a}{M_w Cp_w} + \dfrac{Ky\ a}{h_L\ a}} \left(1 + a_2 \frac{Ky\ a}{h_L\ a} \right) \tag{B.5}$$

$$A_3 = \frac{1}{\dfrac{M_a}{M_w Cp_w} + \dfrac{Ky\ a}{h_L\ a}} \left(a_3 \frac{Ky\ a}{h_L\ a} \right) \tag{B.6}$$

In Eq. (4) the term Hy_i–Hy reduces

$$Hy_i - Hy = b_1 + b_2 T_{wi} + b_3 T_{wi}^3 \tag{B.7}$$

where

$$b_1 = \frac{1}{\dfrac{M_a}{M_w Cp_w} + \dfrac{Ky\ a}{h_L\ a}} \left(a_1 \frac{M_a}{M_w Cp_w} + Hy_1 \frac{M_a}{M_w Cp_w} + T_{w_1} \right) \tag{B.8}$$

$$b_2 = \frac{1}{\dfrac{M_a}{M_w Cp_w} + \dfrac{Ky\ a}{h_L\ a}} \left(b_1 \frac{M_a}{M_w Cp_w} - 1 \right) \tag{B.9}$$

$$b_3 = \frac{1}{\dfrac{M_a}{M_w Cp_w} + \dfrac{Ky\ a}{h_L\ a}} \left(a_3 \frac{M_a}{M_w Cp_w} \right) \tag{B.10}$$

Similarly, the term dHy in Eq. (4) is expressed as a function of dT_{wi} by taking derivative of Eq. (B.3), which gives

$$dHy = (c_2 + c_3\ T_{wi}) dT_{wi} \tag{B.11}$$

where

$$c_2 = \frac{1}{\dfrac{M_a}{M_w Cp_w} + \dfrac{Ky\ a}{h_L\ a}} \left(1 + a_2 \frac{Ky\ a}{h_L\ a} \right) \tag{B.12}$$

$$c_3 = \frac{2}{\dfrac{M_a}{M_w Cp_w} + \dfrac{Ky\ a}{h_L\ a}} \left(a_3 \frac{Ky\ a}{h_L\ a} \right) \tag{B.13}$$

Eq. (5) can then be integrated using the following integrals

$$\int \frac{dx}{a + bx + cx^2} = \frac{2}{\sqrt{4ac - b^2}} \tan^{-1} \frac{2cx + b}{\sqrt{4ac - b^2}} \tag{B.14}$$

where $a = b_1/c_2$, $b = b_2/c_2$, $c = b_3/c_2$

$$\int \frac{x\,dx}{a + bx + cx^2} = \frac{1}{2c} \ln(a + bx + cx^2) - \frac{b}{2c} \int \frac{dx}{a + bx + cx^2} \tag{B.15}$$

where $a = b_1/c_3$, $b = b_2/c_3$, $c = b_3/c_3$.

Symbols

a	—	Specific area in the absorption and humidification column, m^2/m^3
A_c	—	Heat transfer area of the condenser, m^2
AF	—	Absorption factor, $M_w/(m\ M_a)$, dimensionless
Cp	—	Specific heat at constant pressure, kJ/kg K
D	—	Diameter, m
H	—	Absolute humidity, kg H_2O/kg dry air
H^*	—	Absolute humidity at saturation conditions, kg H_2O/kg dry air
Hy	—	Air enthalpy, kJ/kg
Hy^*	—	Air enthalpy at saturation conditions, kJ/kg
H_{OG}	—	Height of transfer units, m
h	—	Heat transfer coefficient, kW/m^2 °C
$h_L a$	—	Heat transfer coefficient at the air water interface, kW/m^2 °C
k	—	Thermal conductivity of condenser tubes, kW/m°C
$kx'a$	—	Mass transfer coefficient of SO_2 in the liquid phase, kg mole SO_2/s m^3
$ky'a$	—	Mass transfer coefficient of SO_2 in the gas phase, kg mole SO_2/s m^3
$Ky\ a$	—	Mass transfer coefficient water vapor in air, kg/(s m^3)
m	—	Slope of equilibrium line, mole fraction in gas/mole fraction in liquid
M	—	Mass flow rate, kg/s
$\overline{M}$	—	Molecular weight, kg/kg mole
N_{OG}	—	Number of transfer units, dimensionless

p — Pressure, kPa
p^* — Saturation pressure, kPa
P — Plant power, MW
r — Condenser tube radius, m
S — Cross section area of the absorption column, m^2
T — Temperature, °C
U_c — Overall heat transfer coefficient in the condenser, $kW/(m^2 K)$
z — Height of absorption or humidification column, m

Greek symbols

λ — Latent heat of water evaporation, kJ/kg

Subscripts

1 — Subscript of streams at the base of humidification or absorption column
2 — Subscript of streams at the top of the humidification or absorption column
3 — Subscript of streams at the top of the condenser
4 — Subscript of streams at the base of the condenser
a — Air
c — Condenser
d — Dehumidifier
cw — Cooling water in the condenser
h — Humidifier
i — Interface between air and water
pw — Product water
v — Water vapor
w — Water
wi — Interface of water and air

References

[1] The 19th IDA worldwide desalting plant inventory, International desalination association, Topsfield, MA, USA, 2006.
[2] S. Parekh, M.M. Farid, J.R. Selman and S.A. Al Hallaj, Solar desalination with a humidification-dehumidification technique - a comprehensive technical review, Desalination, 160 (2004) 168.
[3] S. Al-Hallaj, S. Parekha, M.M. Farid and J.R. Selman, Solar desalination with humidification–dehumidification cycle: Review of economics, Desalination, 195 (2006) 169–186.
[4] G. Yuan and H. Zhang, Mathematical modeling of a closed circulation solar desalination unit with humidification–dehumidification, Desalination, 205 (2007) 156–162
[5] C. Yamali and I. Solmus, Theoretical investigation of a humidification dehumidification desalination system configured by a double-pass flat plate solar air heater Desalination, 205 (2007) 163–177.
[6] C. Yamali and I. Solmus, A solar desalination system using humidification dehumidification process: experimental study and comparison with the theoretical results, Desalination, 220 (2008) 538–551.
[7] J. Orfi, N. Galanis and M. Laplante, Air humidification–dehumidification for a water desalination system using solar energy, Desalination, 203 (2007) 471–481.
[8] H. Marmouch, J. Orfi and S. Ben Nasrallah, Effect of a cooling tower on a solar desalination system, Desalination, 238 (2009) 281–289.
[9] I. Houcine, M. Ben Amara, A. Guizani and M. Maalej, Pilot plant testing of a new solar desalination process by a multiple-effect-humidification technique, Desalination, 196 (2006) 105–124.
[10] T. Tahri, S.A. Abdul-Wahab, A. Bettahar, M. Douani, H. Al-Hinai and Y. Al-Mulla, Desalination of seawater using a humidification-dehumidification seawater greenhouse, Desalin. Water Treat., 12 (2009) 382–388.
[11] A.H. El-Shazly, M.E. El-Gohary and M.E. Ossman, Performance characteristics of a solar humidification dehumidification unit using packed bed of screens as the humidifier, Desalin. Water Treat., 16(2010) 17–28.
[12] G. Prakash Narayan, Mostafa H. Sharqawy, John H. Lienhard V. and Syed M. Zubair, Thermodynamic analysis of humidification–dehumidification desalination cycles, Desalin. Water Treat., 16 (2010) 339–353.
[13] S. Farsad, A. Behzadmehr and S.M. Hosseini Sarvari, Numerical analysis of solar desalination using humidification–dehumidification cycle, Desalin. Water Treat., 19 (2010) 294–300.
[14] Xinghua, Li, Shanker Muraleedaaran, Liangxiong Li and Robert Lee, A humidification-dehumidification process for produced water purification, Desalin. Water Treat., 20 (2010) 51–59.
[15] S.M. Soufari, M. Zamen and M. Amidpour, Experimental validation of an optimized solar humidification-dehumidification desalination unit, Desalin. Water Treat., 6 (2009) 244–251.
[16] E. Mathioulakis, G. Panaras and V. Belessiotis, Experience gained through the implementation and operation of a solar humidification–dehumidification desalination plant, Desalin. Water Treat., 21 (2010) 375–381.
[17] O.K. Bockman, Removal of sulfur dioxide from flue gases by absorption in seawater, Eng. Int. Scan. Congr. Chem. Eng., II (1974) 1–11.
[18] R. Baty, J. Coughlan and S.K. Reynolds, Technical and environmental implications of desulfurization by seawater, I. Chem. E. Sym. Ser., 123 (1990) 143–157.
[19] S.O. Strommen and F. Hjelm, Sulfur in flue gases can safely be absorbed by seawater and return to the oceans, I. Chem. E. Sym. Ser., 131 (1993) 95–108.
[20] J.Z. Abrams, S.J. Zaczek, A.D. Benz, L. Awerbuch and J. Hadinger, Use of seawater in flue gas desulfurization: A new low cost FGD system for special applications, JAPCA, Int. Air Pollution Control Hazardous Waste Manage., 38 (1988c) 969–974.
[21] K. Oikawa, C. Yongsiri, K. Takeda and T. Harimoto, Seawater flue gas desulfurization: Its technical implications and performance results, Environmental Progress, 22 (2003) 67–73.
[22] Y. Zhao, S. Ma, X. Wang and Q. Zhang, Experimental and mechanism studies on seawater flue gas desulfurization, J. Environ. Sci., 15 (2003) 123–128.
[23] F.J. Gutiérrez Ortiz, F. Vidal, P. Ollero, L. Salvador and V. Cortés, Pilot-Plant Technical Assessment of Wet Flue Gas Desulfurization Using Limestone, Ind. Eng. Chem. Res., 45 (2006) 1466–1477.
[24] F. Vidal B., P. Ollero, F.J. Gutiérrez Ortiz and A. Villanueva, Catalytic Seawater Flue Gas Desulfurization Process: An Experimental Pilot Plant Study, Environ. Sci. Technol., 41(20) (2007) 7114–7119.
[25] J. Cohen, I. Janovich and A. Muginstein, Utilization of waste heat from a flue gases up-stream gas scrubbing system, Desalination, 139 (2001) 1–6.
[26] Corrado Sommarva, Utilisation of power plant waste heat steams to enhance efficiency in thermal desalination, Desalination, 222 (2008) 592–595.

[27] D. Dajnak and F.C. Lockwood, Use of thermal energy from waste heat for seawater desalination, Desalination, 130 (2000) 137–146.
[28] A.H. Abdulsattar, S. Sridhar and L.A..Bromley, Thermodynamics of the Sulfur Dioxide-Seawater System, AIChE J., 23 (1977) 62–68.
[29] G. Pipitone and O. Bolland, Modeling of oxy-combustion flue gas desulfurization by seawater absorption, Environ. Prog. Sustainable Energy, 28 (2009) 20–29.
[30] M. Radojevic, The use of seawater for flue gas desulphurization, Environmental Technology Letters, 10 (1989) 71–76.
[31] K. Oikawa, C. Yongsiri, K. Takeda and T. Harimoto, Seawater flue gas desulfurization: Its technical implications and performance results, Environ. Prog., 22 (2003) 67–73.
[32] Yi Zhao, Shuang-Chen Ma, Xiao-Ming Wang and Qing Zhang, Experimental and mechanism studies on seawater flue gas desulfurization, J. Environ. Sci., 15 (2003) 123–128.
[33] Nyman and B.G. Goran, Seawater scrubbing removes SO_2 from refinery flue gases Oil and Gas Journal, 89 (1991) 51–55.
[34] R.P. Whitney and J.E. Vivian, Absorption of SO_2 in water, Chem. Eng. Prog., 45 (1949) 323.
[35] A.S. Foust, L.A. Wenzel, C.W. Clump, L. Maus and L.B. Andresen, Principles of Unit Operation, 2nd edt., Wiley, 1980, NJ, USA.
[36] M.M. Farid, Sandeep Parekh, J.R. Selman and Said Al-Hallaj, Solar desalination with a humidification-dehumidification cycle: mathematical modeling of the unit, Desalination, 151 (2002) 153–164.
[37] N.K. Nawayseh, M.M. Farid, S. Al-Hallaj and A. Al-Timimi, Solar desalination based on humidification process – I. Evaluating the heat and mass transfer coefficients, Energy Conversion & Management, 40 (1999) 1423–1439.
[38] G.F. Hewitt, Heat Exchanger Design Handbook, Begelle House Inc., New York, 1998.
[39] M. Al-Sahali and H.M. Ettouney, Humidification dehumidification desalination process: Design and performance evaluation, Chem. Eng. J., 143 (2008) 257–264.
[40] M.H. Sharqawya, J.H. Lienhard V and S.M. Zubair, Thermophysical properties of seawater: a review of existing correlations and data, Desalin. Water Treat., 16 (2010) 354–380.